

# Retromer facilitates the localization of Bcl-xL to the mitochondrial outer membrane

Trey Farmer<sup>a</sup>, Katelyn L. O'Neill<sup>b</sup>, Naava Naslavsky<sup>a</sup>, Xu Luo<sup>b</sup>, and Steve Caplan<sup>a,b,\*</sup>

<sup>a</sup>Department of Biochemistry and Molecular Biology and <sup>b</sup>Eppley Institute for Research in Cancer and Allied Diseases, The Fred and Pamela Buffett Cancer Center, University of Nebraska Medical Center, Omaha, NE 68198-5870

**ABSTRACT** The anti-apoptotic Bcl-2 family protein Bcl-xL plays a critical role in cell survival by protecting the integrity of the mitochondrial outer membrane (MOM). The mechanism through which Bcl-xL is recruited to the MOM has not been fully discerned. The retromer is a conserved endosomal scaffold complex involved in membrane trafficking. Here we identify VPS35 and VPS26, two core components of the retromer, as novel regulators of Bcl-xL. We observed interactions and colocalization between Bcl-xL, VPS35, VPS26, and MICAL-L1, a protein involved in recycling endosome biogenesis that also interacts with the retromer. We also found that upon VPS35 depletion, levels of nonmitochondrial Bcl-xL were increased. In addition, retromer-depleted cells displayed more rapid Bax activation and apoptosis. These results suggest that the retromer regulates apoptosis by facilitating Bcl-xL's transport to the MOM. Importantly, our studies suggest a previously uncharacterized relationship between the machineries of cell death/survival and endosomal trafficking.

## Monitoring Editor

Thomas D. Fox  
Cornell University

Received: Jan 22, 2019

Revised: Feb 25, 2019

Accepted: Mar 1, 2019

## INTRODUCTION

Apoptosis is essential for normal development and the maintenance of tissue homeostasis, protection from genomic instability, and the control of humoral immune responses (Slomp and Peperzak, 2018). The Bcl-2 protein family is composed of crucial regulators of apoptosis that can be divided into proapoptotic (Bax, Bak, Bad, etc.) or anti-apoptotic (Bcl-2, Bcl-xL, Mcl-1, A1, etc.) proteins (Farrow and Brown, 1996; Fuchs and Steller, 2015; Adams and Cory, 2018). On

one hand, interference with key apoptotic regulators may lead to uncontrolled cell growth and pathologies that include breast (Placzek *et al.*, 2010; Tawfik *et al.*, 2012) and lung (Han *et al.*, 2002; Viard-Leveugle *et al.*, 2003) cancer, as a result of compromised cell death pathways. On the other hand, overactive cell death pathways can lead to neurodegenerative disorders such as Alzheimer's (Lee *et al.*, 2010; Crews *et al.*, 2011) and Parkinson's (Berry *et al.*, 2010; Barcia *et al.*, 2011) disease. Bcl-xL, a vital anti-apoptotic protein, is up-regulated in a variety of cancers, and increases resistance to cell death (Choi *et al.*, 2016; Scherr *et al.*, 2016). Although Bcl-xL functions through a number of mechanisms, a key mode of its action is via the sequestration of the proapoptotic proteins Bax and Bak, thus preventing pore formation in the mitochondrial outer membrane (MOM) and the subsequent release of cytochrome *c* and caspases that trigger downstream death signals (Oltvai *et al.*, 1993; Shimizu *et al.*, 1995; Yang *et al.*, 1995). Bcl-xL is mainly found on the MOM, but also partially localizes to the cytoplasm (Hsu *et al.*, 1997; Hausmann *et al.*, 2000; Nijhawan *et al.*, 2003). Although not well defined, certain cellular signals result in Bcl-xL translocation to the MOM (Hsu *et al.*, 1997), suggesting that Bcl-xL transport from the cytoplasm to the mitochondria could be an important regulatory step in the apoptotic cascade. Clues to the mechanism by which Bcl-xL translocates to the MOM are derived from previous studies addressing the translocation of other Bcl-2 family members. Because Bax undergoes diffusion from the cytoplasm to the mitochondrial membrane (Wolter *et al.*, 1997), given its homology with Bcl-xL, one possibility is that the latter protein reaches mitochondria in a

This article was published online ahead of print in MBoC in Press (<http://www.molbiolcell.org/cgi/doi/10.1091/mbc.E19-01-0044>) on March 6, 2019.

The authors declare no conflicts of interest.

Author contributions: T.F. created reagents, carried out experiments, analyzed data, prepared figures, and wrote parts of the manuscript. K.L.O. created reagents and analyzed data. N.N. guided experimentation, analyzed data, and edited parts of the manuscript. X.L. guided experimentation, analyzed data, edited the manuscript, and codirected the study. S.C. guided experimentation, analyzed data, prepared figures, and directed the study.

\*Address correspondence to: Steve Caplan ([scaplan@unmc.edu](mailto:scaplan@unmc.edu)).

Abbreviations used: ATCC, American Type Culture Collection; BSA, bovine serum albumin; DRP1, dynamin-related protein 1; EHD1, Eps15 homology domain-containing protein 1; FBS, fetal bovine serum; IB, immunoblotting; IF, immunofluorescence; IP, immunoprecipitation; mCh-Tom20, mCherry-tagged Tom20 N-terminal 10 residues; MOM, mitochondrial outer membrane; PBS, phosphate-buffered saline; PBST, phosphate-buffered saline plus 0.3% Tween; RPE1, retinal pigment epithelium; siRNA, small interfering RNA; Z-VAD, Z-valine-alanine-aspartic acid-(OMe)-fluoromethylketone.

© 2019 Farmer *et al.* This article is distributed by The American Society for Cell Biology under license from the author(s). Two months after publication it is available to the public under an Attribution–Noncommercial–Share Alike 3.0 Unported Creative Commons License (<http://creativecommons.org/licenses/by-nc-sa/3.0>).

"ASCB®," "The American Society for Cell Biology®," and "Molecular Biology of the Cell®" are registered trademarks of The American Society for Cell Biology.

mechanism similar to Bax, relying primarily on diffusion. However, few studies have directly addressed the mechanism by which cytoplasmic Bcl-xL is targeted to the MOM.

In addition to diffusion as a potential mechanism for Bcl-2 family members to reach the MOM, other mechanisms of transport might also contribute to this translocation. Indeed, one possibility is that endocytic membrane trafficking might account for some of the Bcl-xL movement to the MOM. Although endocytic trafficking is primarily responsible for regulating the internalization of proteins and lipids from the plasma membrane and their recycling (Naslavsky and Caplan, 2018), recent studies have implicated endocytic membrane trafficking in a variety of nonendocytic cellular events, including mitochondrial fission (Lee *et al.*, 2016; Farmer *et al.*, 2017) and centriole disengagement/duplication (Xie *et al.*, 2018). For example, the Eps15 homology domain-containing protein 1 (EHD1), a key regulator of receptor recycling to the plasma membrane (Caplan *et al.*, 2002; Guilherme *et al.*, 2004), regulates both mitochondrial fission and centriole disengagement (Xie *et al.*, 2018). Moreover, the endocytic scaffolding complex known as the retromer, composed of the core subunits VPS26, VPS29, and VPS35, and two sorting nexin proteins, has also been implicated in mitochondrial fission (Tang *et al.*, 2015; Wang *et al.*, 2016, 2017; Farmer *et al.*, 2017, 2018; Naslavsky and Caplan, 2018) and centriole disengagement (Xie *et al.*, 2018). The VPS35 subunit also directly interacts with and regulates several mitochondrial fission and fusion factors, including the E3 ligase Mul1 (Braschi *et al.*, 2010; Tang *et al.*, 2015) and the fission factor, dynamin-related protein-1 (DRP1; Tang *et al.*, 2015; Wang *et al.*, 2016, 2017; Farmer *et al.*, 2017). Interestingly, Bcl-xL and DRP1 interact and colocalize on clathrin-associated vesicles (Li *et al.*, 2013), suggesting potential control of Bcl-xL by endocytic regulatory proteins. Accordingly, we have hypothesized that VPS35 and the retromer might interact with Bcl-xL and influence apoptosis.

Herein, we address whether the retromer and endocytic trafficking directs Bcl-xL translocation from the cytoplasm to the MOM. We demonstrate for the first time that Bcl-xL physically interacts with VPS35 and retromer subunits in a DRP1-independent manner. Moreover, the retromer and Bcl-xL colocalize on vesicles that are distinct from mitochondria. Significantly, the depletion of VPS35 from cells both reduces mitochondrial-localized Bcl-xL, and increases the rate of staurosporine-induced apoptosis. Although only a portion of Bcl-xL may rely on retromer for transport to the MOM, given the significance of this protein in the regulation of apoptosis, this previously uncharacterized pathway for the delivery of Bcl-xL to the mitochondrial membrane may have potentially significant consequences.

## RESULTS AND DISCUSSION

### Bcl-xL resides in a protein complex with endocytic proteins and DRP1

Bcl-xL localizes to the MOM where it modulates apoptosis, but a pool of the protein is also observed in the cytoplasm (Hsu *et al.*, 1997; Hausmann *et al.*, 2000; Nijhawan *et al.*, 2003). Evidence supports a diffusion mechanism for some Bcl-2 family members from the cytoplasm to the MOM, where the proteins are subsequently immobilized (Wolter *et al.*, 1997). For example, conformational changes and homo-oligomerization of Bax lead to the exposure of mitochondrial targeting sequences within four of the protein's nine helices (George *et al.*, 2010). However, despite Bcl-xL's crucial role in inhibiting apoptosis and the potential significance of its translocation, the specific mechanisms of Bcl-xL targeting to the MOM remain poorly understood. Recent studies demonstrate the involvement of membrane trafficking complexes in protein delivery to the MOM (Tang *et al.*, 2015; Wang *et al.*, 2016; Farmer *et al.*, 2018);

accordingly, we hypothesized that Bcl-xL might also, in part, be regulated by endocytic membrane trafficking pathways.

We first tested whether Bcl-xL could be found in a complex with endocytic regulatory proteins. Given the known interactions between Bcl-xL and DRP1 (Li *et al.*, 2013), and between DRP1 and the retromer complex (Wang *et al.*, 2016, 2017), and the increasing number of trafficking pathways mediated by the retromer (Tang *et al.*, 2015; Wang *et al.*, 2016; Farmer *et al.*, 2018), we tested for an interaction between Bcl-xL and the retromer complex. As demonstrated, antibodies to VPS26 pulled down detectable levels of the ~37 kDa endogenous VPS26 protein (Figure 1A; low and medium exposures), as well as endogenous DRP1 (Figure 1A; high exposure) and endogenous Bcl-xL (Figure 1A; low and medium exposures). Antibodies to Bcl-xL pulled down the Bcl-xL protein (Figure 1A; low and medium exposures), as well as VPS26 (Figure 1A; low and medium exposures) and DRP1 (high exposure), whereas control immunoglobulins (Ctl) did not precipitate any detectable VPS26, DRP1, or Bcl-xL. Moreover, immunoprecipitation with antibodies to MICAL-L1, an endocytic regulatory protein that interacts with the retromer (Zhang *et al.*, 2012), also precipitated Bcl-xL in addition to the retromer subunits (Figure 1B). These data support the notion that Bcl-xL partially resides in a complex containing the retromer.

Because DRP1 interacts with both Bcl-xL (Li *et al.*, 2013) and the retromer complex (Li *et al.*, 2013), we next asked whether DRP1 links Bcl-xL to the retromer. To address this question, we used small interfering RNA (siRNA) to deplete cells of DRP1 (Figure 1C, quantified in D), and then used the DRP1-depleted lysate for coimmunoprecipitations with anti-Bcl-xL antibodies. As expected, Bcl-xL precipitated itself in Mock- and DRP1-depleted lysates (Figure 1E, bottom panel, quantified in F). However, similar to the Mock-treated cells, both the retromer VPS26 and VPS35 subunits could nonetheless be precipitated by Bcl-xL in the DRP1-depleted cells (Figure 1E, top and middle panels, quantified in F). Similarly, siRNA knockdown of VPS35 (Supplemental Figure 1A), did not prevent the pull down of DRP1 by Bcl-xL (Supplemental Figure 1B). Overall, these data support the idea that Bcl-xL interacts with the retromer complex in a DRP1-independent manner.

### Bcl-xL localizes to endocytic vesicles containing the retromer

Because Bcl-xL interacts with several subunits of the retromer complex, we hypothesized that the retromer may serve as a mechanism for the translocation of a subset of cytoplasmic Bcl-xL to the MOM. Given that the ratio of Bcl-xL in the cytoplasm versus MOM-bound Bcl-xL does not significantly change under apoptotic conditions (Wolter *et al.*, 1997), any contribution to the balance of mitochondrial-to-cytoplasmic Bcl-xL might be physiologically relevant. Accordingly, we rationalized that if a portion of cytoplasmic Bcl-xL is translocated to the MOM in a retromer-dependent process, we would anticipate visualizing vesicles containing retromer subunits together with Bcl-xL. To test this idea, we transfected RPE1 cells with the mCherry-tagged Tom20 N-terminal 10 residues as a marker of the mitochondrial membrane, and then immunostained the cells with antibodies directed against endogenous Bcl-xL and VPS26 (Figure 2 and see three-dimensional [3D] rotation in Supplemental Figure 2 and Supplemental Video 1). As demonstrated, populations of Bcl-xL were observed on vesicles that also contained VPS26 (Figure 2, A, inset in B, E, and H), and these vesicles were almost entirely devoid of the Tom20 MOM marker. However, most of the Bcl-xL colocalized with the mitochondrial Tom20, and was devoid of VPS26 (Figure 2A and inset in C, E, and F). Indeed, quantification showed that ~65% of

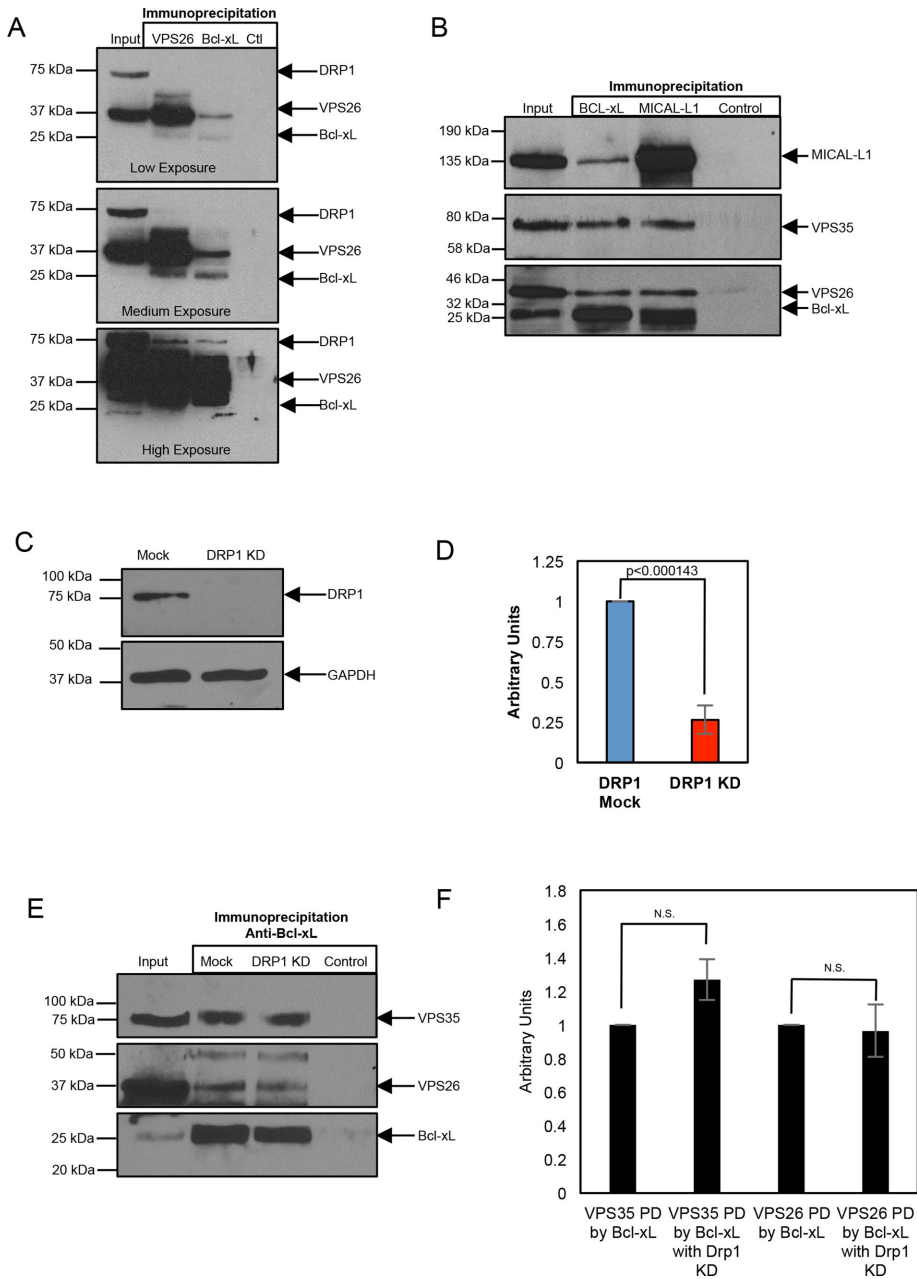


**FIGURE 1:** Bcl-xL resides in a protein complex with members of the retromer and DRP1. (A) HeLa cell lysates were subjected to immunoprecipitations with anti-VPS26, anti-Bcl-xL, or control IgG, and immunoblotted with antibodies against Drp1, VPS26, and Bcl-xL. Three different exposures of the same immunoblot are depicted: low, medium, or high exposure. Gels depicted are representative of three independent experiments showing similar results. Densitometric analysis from these experiments shows that 1) compared with the level of VPS26 precipitated with anti-VPS26 (defined as 100%), 41–66% of VPS26 precipitates with anti-Bcl-xL, and 2) the level of DRP1 precipitated by anti-Bcl-xL ranges from ~50 to 90% of that precipitated by anti-VPS26. (B) HeLa cell lysates were subjected to immunoprecipitations with anti-Bcl-xL, anti-MICAL-L1, or control IgG, and immunoblotted with antibodies against MICAL-L1, VPS35, VPS26, and Bcl-xL. Gel depicted is representative of three individual experiments showing similar results. Densitometric analysis from these experiments shows that 1) the ratio of VPS26:Bcl-xL precipitated with anti-Bcl-xL is  $0.660 \pm 0.110$ , which is very similar to the ratio of VPS35:Bcl-xL precipitated with anti-Bcl-xL ( $0.6866 \pm 0.169$ ), and 2) the ratio of VPS26:MICAL-L1 precipitated with anti-MICAL-L1 ( $0.589 \pm 0.215$ ) is similar to the ratio of VPS35:MICAL-L1 precipitated with anti-MICAL-L1 ( $0.607 \pm 0.129$ ). (C) Efficacy of DRP1 depletion is demonstrated by immunoblotting lysates from Mock- or DRP1-depleted HeLa cells with anti-DRP1, and using GAPDH as a loading control. (D) Densitometric quantification of DRP1 protein levels in either Mock- or DRP1-siRNA treatment. Error bars denote SD. *p* values were determined by the Student's one-tailed *t* test. *n* = 3. (E) HeLa cells were treated with either

the Bcl-xL was localized to mitochondria, and <30% was observed with VPS26 (Figure 2D). Moreover, endogenous VPS35 displayed nearly 85% overlap with VPS26 as expected, and like VPS26, VPS35 showed a similar degree of colocalization with Bcl-xL at ~25% (Supplemental Figure 3). In addition, nearly 20% of the Bcl-xL overlapped with Rab5, another resident of sorting endosomes, but little or no colocalization was observed with endosomal EEA1 (Supplemental Figure 4). These data illustrate for the first time that a pool of Bcl-xL localizes to a subset of endosomal vesicles that contain retromer and Rab5, suggesting the possibility that the retromer transports a fraction of Bcl-xL to the MOM.

### Loss of VPS35 or MICAL-L1 results in increased nonmitochondrial Bcl-xL

The retromer is a scaffold and endocytic membrane complex responsible for the trafficking of a variety of proteins including the mannose 6-phosphate receptor, iron transporter DMT1-11/Slc11a2, and the Wnt transport protein Wntless/MIG-14 (Arighi *et al.*, 2004; Eaton, 2008; Tabuchi *et al.*, 2010). In each case, interference with retromer function leads to mislocalization (Eaton, 2008; Tabuchi *et al.*, 2010) or occasionally to reduced expression levels of its cargo, possibly due to degradation (Arighi *et al.*, 2004).

To determine the effect of retromer on Bcl-xL localization, we treated cells with siRNA specific for either VPS35, or the retromer interaction partner MICAL-L1, and compared the amount of nonmitochondrial Bcl-xL in these cells to Mock-treated cells (Figure 3). Knockdown of VPS35 had no effect on the total level of Bcl-xL (Supplemental Figure 5). However, whereas in Mock-treated cells the majority of the Bcl-xL localized to Tom20-marked MOM (Figure 3A, top panel, quantified in B), upon depletion of either VPS35 or MICAL-L1 (Figure 3, C and D), significantly more nonmitochondrial Bcl-xL was observed (Figure 3A, middle and bottom panels [Bcl-xL in red], quantified in B). Moreover, VPS35 knockdown led to an

Mock- or DRP1-siRNA, immunoprecipitated with antibodies against Bcl-xL, and immunoblotted with antibodies against VPS35, VPS26, and Bcl-xL. Gel depicted is representative of three individual experiments showing similar results. (F) Densitometric quantification of VPS35 or VPS26 protein levels immunoprecipitated by anti-Bcl-xL in the presence or absence of DRP1. Error bars denote SD. *p* values were determined by the Student's one-tailed *t* test. *n* = 3.

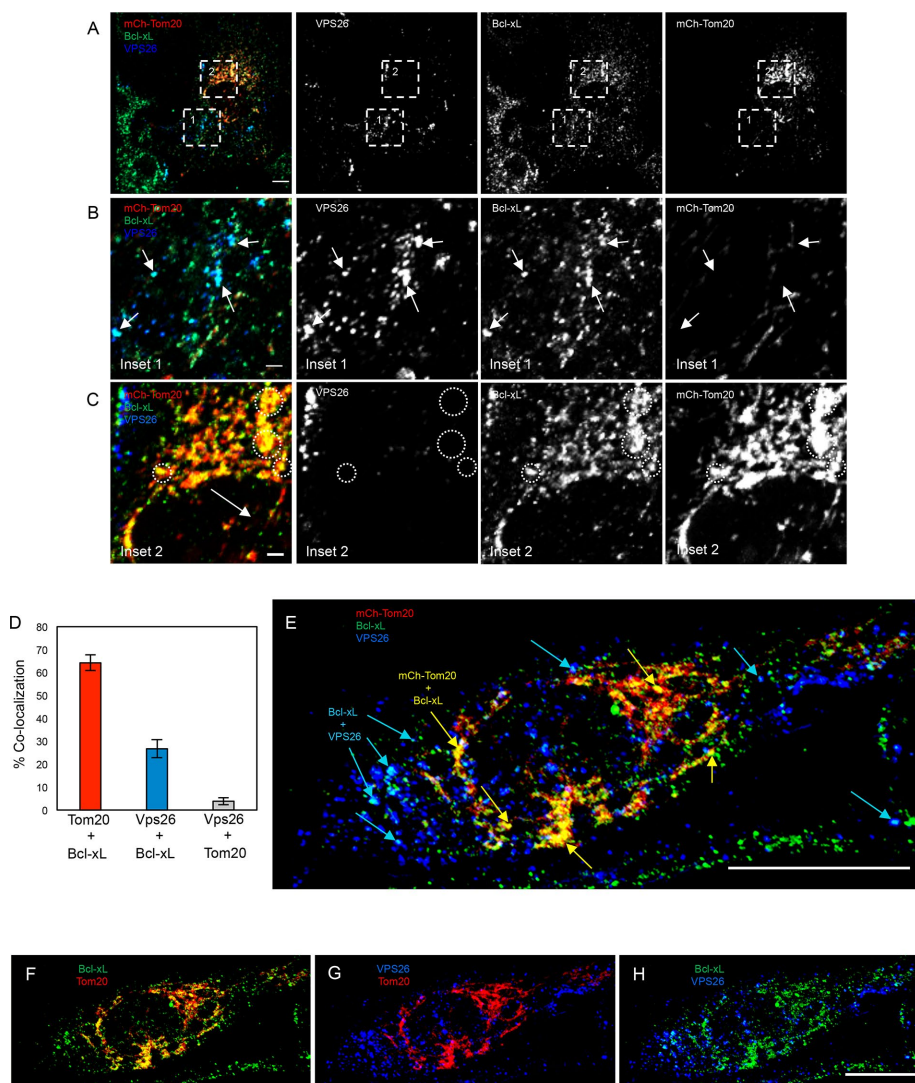


**FIGURE 2:** Bcl-xL localizes to endocytic vesicles containing the retromer. (A) RPE1 cells were transfected with the N-terminal 10 residues of the mitochondrial outer membrane protein (Tom20) tagged with mCherry (mCh-Tom20; red), and immunostained with VPS26 (blue) and Bcl-xL (green). Images shown are 3D snapshots of serial z-sections. Channels were split, showing the individual protein localization patterns (right panels). Regions of interest are highlighted with dashed boxes labeled as 1 or 2, and they correspond to the inset images depicted in B and C. Scale bar = 10  $\mu$ m. (B) Inset area 1 from A. Arrows denote vesicles containing VPS26 (blue) and Bcl-xL (green) but lack mCh-Tom20 (red). Channels were split, showing the individual protein localizations. Scale bar = 2  $\mu$ m. (C) Inset area 2 from A. Dashed circles show areas where Bcl-xL (green) is colocalized with mCh-Tom20 (red), but not VPS26 (blue). Channels were split, showing the individual protein localizations. Scale bar = 2  $\mu$ m. Images portrayed are representative of three independent experiments (quantified in D). (D) The colocalization threshold analysis tool in Fiji ImageJ was used to quantify the colocalization between Bcl-xL and mCh-Tom20, Bcl-xL and VPS26, or mCh-Tom20 and VPS26. Data are presented as a mean, and error bars indicate SD.  $n = 3$ . (E) A single representative RPE1 cell transfected with mCh-Tom20 (red), and immunostained with VPS26 (blue) and Bcl-xL (green). The image shown is a 3D snapshot of serial z-sections. Blue arrows depict VPS26 and Bcl-xL colocalization, whereas yellow arrows depict Bcl-xL and Tom20 colocalization. Scale bar = 10  $\mu$ m. (F–H) Individual two-channel images from E are shown depicting the colocalization between Tom20 and Bcl-xL (F), VPS26 and Tom20 (G), and between Bcl-xL and VPS26 (H).

increased ratio of nonmitochondrial Bcl-xL, as determined by immunoblotting mitochondrial enriched fractions (Figure 3E, quantified in F). Given that the nonmitochondrial Bcl-xL does not appear to colocalize with any endocytic or membrane markers that we tested (unpublished observations), and given the propensity for Bcl-xL to

VPS35-siRNA and were either given no treatment, or treated with staurosporine (Figure 4, A and B; Belmokhtar *et al.*, 2001). Efficacy of the siRNA depletion was verified in Figure 4C. All cells were also treated with Z-valine-alanine-aspartic acid-(OMe)-fluoromethylketone (Z-VAD) to prevent the cells from undergoing complete

oligomerize (Basanez *et al.*, 2001; O'Neill *et al.*, 2006), it is possible that the Bcl-xL remains in cytoplasmic aggregates. Indeed, Bcl-xL homodimers have been observed in the cytoplasm (Jeong *et al.*, 2004). Overall, these data lend support for the idea that Bcl-xL is normally translocated from the cytoplasm to the MOM in a mechanism that partially relies on the function of an intact retromer complex, and loss of the retromer leads to increased Bcl-xL presence in the cytoplasm.

### VPS35-depleted cells display an enhanced rate of apoptosis

In nonapoptotic cells, the proapoptotic Bcl-2-family protein Bax is primarily localized to the cytoplasm and there is only a modest presence on the outer MOM (Hsu *et al.*, 1997; Wolter *et al.*, 1997; Griffiths *et al.*, 1999). A key role of the anti-apoptotic Bcl-xL is to sequester Bax in the cytoplasm and prevent its translocation, and/or bind to Bax at the MOM and prevent its function in pore formation (Yang *et al.*, 1995; Manon *et al.*, 1997; Wolter *et al.*, 1997). Another proapoptotic Bcl-2-family protein, Bad, regulates Bcl-xL function by binding to Bcl-xL (Howells *et al.*, 2011), thus allowing Bax access to the MOM and facilitating pore formation, cytochrome c release, and cell death (Goping *et al.*, 1998; Gilmore *et al.*, 2000; Bleicken *et al.*, 2010). Indeed, because MOM-localized Bcl-xL has the ability to inhibit Bax by dissociating oligomers or by preventing Bax insertion into the MOM (Xu *et al.*, 2013; Subburaj *et al.*, 2015), even small fluctuations in Bcl-xL levels at the MOM might have a significant impact on the regulation of apoptosis. Accordingly, we hypothesized that if VPS35 depletion decreases the ratio of Bcl-xL at the MOM compared with cytoplasmic Bcl-xL, this might enhance the rate of apoptosis.

To test whether VPS35 depletion led to an enhanced apoptotic rate, we examined Bax recruitment to the MOM (and to punctate structures that form membrane pores) in the presence and absence of VPS35, upon treatment with the kinase inhibitor and inducer of apoptosis, staurosporine (Figure 4). In these experiments, we used CRISPR/Cas9 gene-edited HCT 116 cells that were depleted of endogenous Bax and Bak, but were stably transfected with GFP-tagged Bax (GFP-Bax; O'Neill *et al.*, 2016). The cells were treated with Mock- or

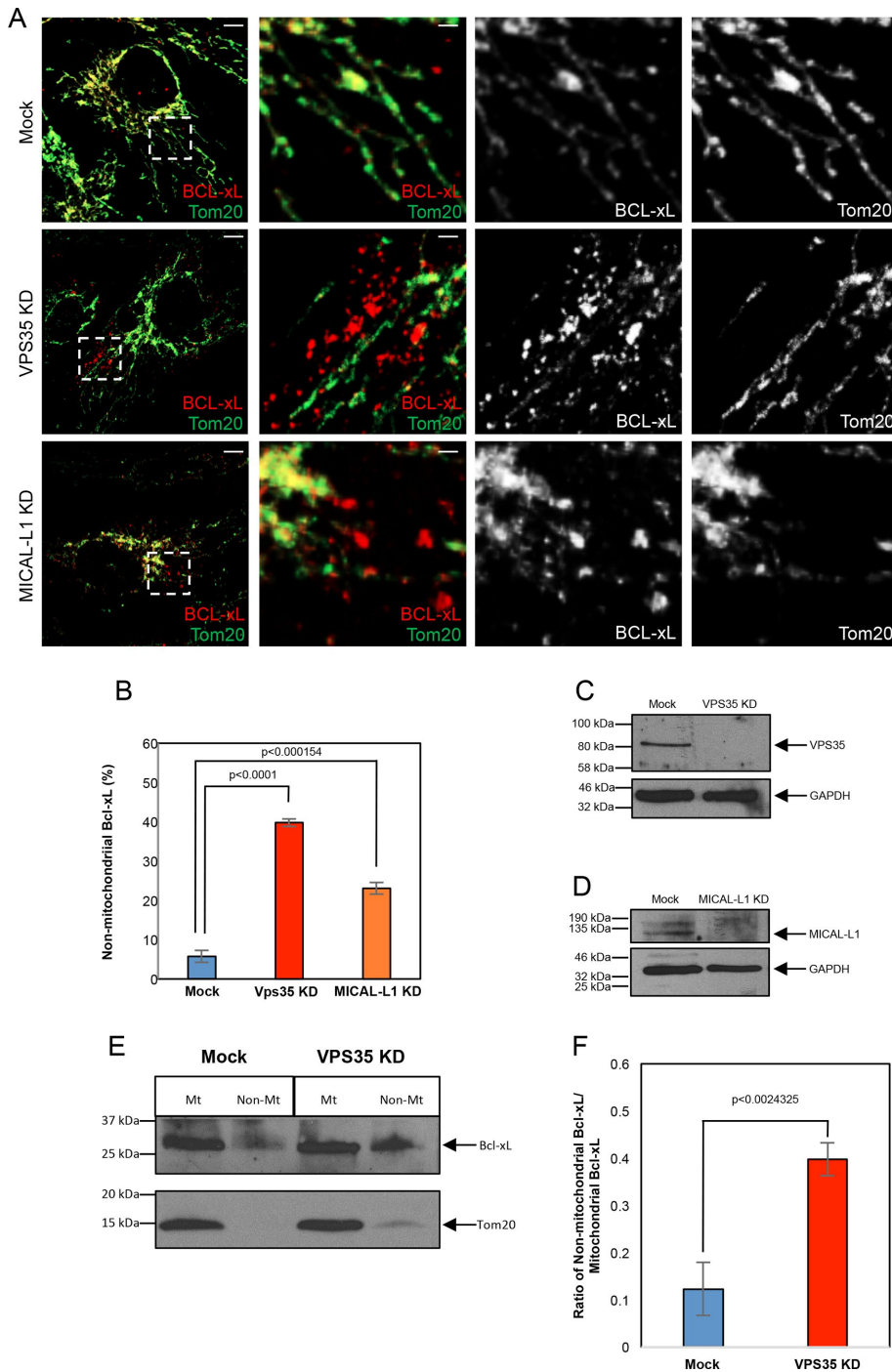


**FIGURE 3:** Loss of VPS35 or MICAL-L1 leads to increased nonmitochondrial Bcl-xL. (A) RPE1 cells were subjected to Mock-, VPS35-, or MICAL-siRNA, immunostained with antibodies against Tom20 (green) and Bcl-xL (red), and serial z-sections were obtained. The images depicted are 3D snapshots. Dashed regions of interest correspond to the insets in the three right-hand panels. Inset channels were split, showing the individual protein localization patterns. Scale bar = 10  $\mu$ m, (2  $\mu$ m; inset). (B) Quantification of the mean number of nonmitochondrial-associated Bcl-xL structures upon Mock-, VPS35-, and MICAL-L1-siRNA treatment. Error bars denote SD. *p* values were determined by the Student's one-tailed *t* test. *n* = 3. (C) Efficacy of the VPS35-depletion is demonstrated by immunoblotting lysates from Mock- or VPS35-depleted RPE1 cells, with GAPDH as a loading control. (D) Efficacy of MICAL-L1-depletion is demonstrated by immunoblotting lysates from Mock- or MICAL-L1-depleted RPE1 cells using GAPDH as a loading control. (E) HeLa cells were treated with either Mock- or VPS35-siRNA, homogenized, and subject to immunofractionation with anti-Tom20 to generate an enriched mitochondrial fraction (Mt) and a nonmitochondrial fraction (Non-Mt). The fractions were separated by SDS-PAGE and immunoblotted with anti-Bcl-xL and anti-Tom20. (F) Densitometric quantification

apoptosis and detachment from the coverslips. As expected, the GFP-Bax in the cells with no staurosporine treatment (with either Mock- or VPS35-siRNA), displayed primarily cytoplasmic GFP-Bax, suggesting a lack of Bax recruitment to the MOM and cells that were nonapoptotic (Figure 4A, left panels). However, upon staurosporine treatment, although both Mock- and VPS35-siRNA-treated cells displayed punctate Bax recruitment to the MOM (indicative of apoptosis), at the 60-min time point significantly more Bax was recruited to the MOM in the VPS35 KD cells (Figure 4A, right panels, quantified in B). To further assess whether the rate of apoptosis was enhanced in the absence of VPS35, we used a Parp1 cleavage apoptosis assay (Kaufmann *et al.*, 1993; Tewari *et al.*, 1995) at three different time points (Figure 4, D and E). Indeed, we observed a more rapid decrease in the level of full-length Parp1 over 30–60 min upon staurosporine treatment in cells lacking VPS35 as compared with Mock-treated cells (Figure 4, D and E). We quantified the loss of full-length Parp1 by measuring the ratio of Parp1:GAPDH (loading control), and found a significant decrease in full-length Parp1 in VPS35-depleted cells after both 30 and 60 min of staurosporine treatment compared with Mock-treated cells (Figure 4E). These data are consistent with the notion that the retromer is partially responsible for Bcl-xL translocation to the MOM, and in its absence, the rate of apoptosis is enhanced.

The tight control that Bcl-xL exerts over Bax-driven pore formation at the MOM and apoptosis hints at the significance of regulating its mitochondrial localization. Despite this, although studies have addressed other Bcl-2-family protein recruitment to MOM (Wolter *et al.*, 1997; Desagher *et al.*, 1999; Eskes *et al.*, 2000) or Bcl-xL insertion into membranes (Hsu *et al.*, 1997; Kaufmann *et al.*, 2003; Schinzel *et al.*, 2004), to date few studies have studied the mechanisms by which it is translocated to the MOM. Our data provide the first evidence that Bcl-xL interacts with the retromer complex and localizes to endocytic vesicles, and we demonstrate that the retromer complex is partially responsible for Bcl-xL localization to the MOM. Our data support a model in which

of the ratio of nonmitochondrial Bcl-xL vs. mitochondrial Bcl-xL in either Mock- or VPS35- siRNA treatment. Error bars denote SD. *p* values were determined by the Student's one-tailed *t* test. *n* = 3.

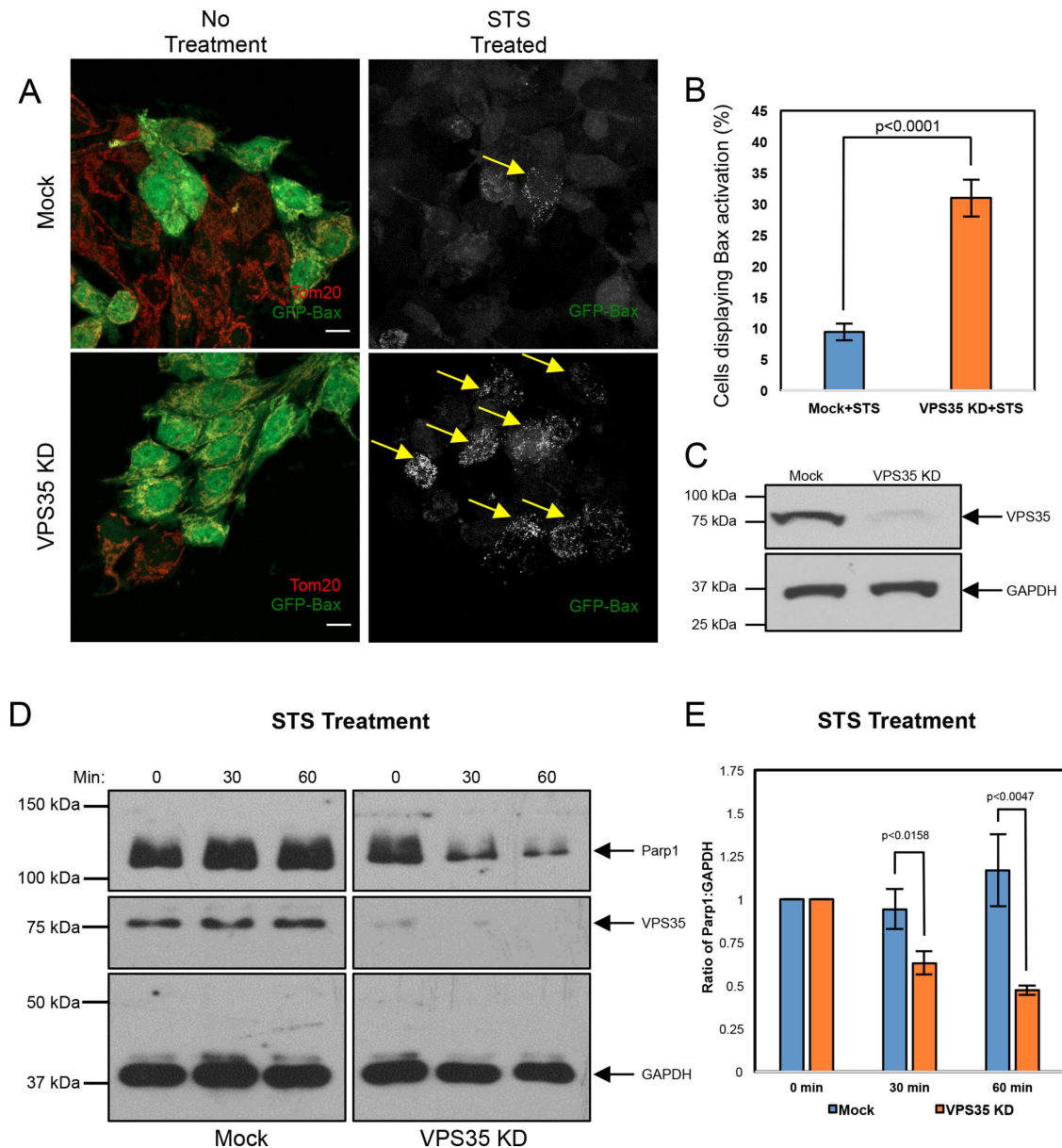


**FIGURE 4:** The rate of Bax activation at the mitochondrial membrane is enhanced in cells lacking VPS35. (A) CRISPR/Cas9 HCT 116 cells lacking endogenous Bak and Bax, but expressing stably transfected GFP-Bax, were subject to Mock- or VPS35-siRNA knockdown, with or without staurosporine (STS) treatment for 60 min. Cells were fixed and immunostained with anti-Tom20 (red). For micrographs representing the STS treatment, only GFP-Bax is shown. Scale bar = 10  $\mu$ m. (B) Quantification of the mean percentage of Mock- or VPS35-siRNA-treated cells displaying GFP-Bax activation upon STS treatment. Error bars represent SD. *p* value was determined by the Student's one-tailed *t* test. *n* = 3. (C) Efficacy of the VPS35-siRNA treatment is demonstrated by immunoblotting lysates from Mock- or VPS35-depleted CRISPR/Cas9 HCT 116 cells with anti-VPS35. GAPDH was used as a loading control. (D) CRISPR/Cas9 HCT 116 cells lacking endogenous Bak and Bax, but expressing stably transfected GFP-Bax, were subject to either Mock- or VPS35-siRNA treatment for 48 h, and treated acutely with STS for 0, 30, or 60 min. Lysates from each treatment were analyzed by immunoblotting for Parp1 to assess cleavage over time, and immunoblotting with anti-VPS35 was used to verify the siRNA treatment efficacy. GAPDH was used as a loading control. (E) Densitometric representation of the data from D was done using ImageJ to calculate the ratio of Parp1:GAPDH between Mock- and VPS35-siRNA-treated cells. Data are presented as a mean, and error bars indicate SD. *p* values were determined by the Student's one-tailed *t* test. *n* = 3.

depletion of the retromer complex subunit VPS35 leads to reduced Bcl-xL at the MOM, causing enhanced Bax-mediated pore formation and Cyt c release upon staurosporine treatment, and an enhanced rate of apoptosis (Figure 5). Overall, our study highlights a novel role for the retromer, an endosomal protein complex, in the localization of Bcl-xL to the MOM, thus forging a link between endocytic regulation and apoptosis.

## MATERIALS AND METHODS

### Reagents and antibodies

Staurosporine was purchased from Sigma Aldrich (S5921). Z-VAD was purchased from Fisher Scientific (MP Biomedical; MP3FK00901). Commercial antibodies with their specific use (IB, immunoblotting; IF, immunofluorescence; and IP, immunoprecipitation) and catalogue numbers are indicated. Anti-VPS26 (IB, IF, IP, ab23892), anti-VPS35

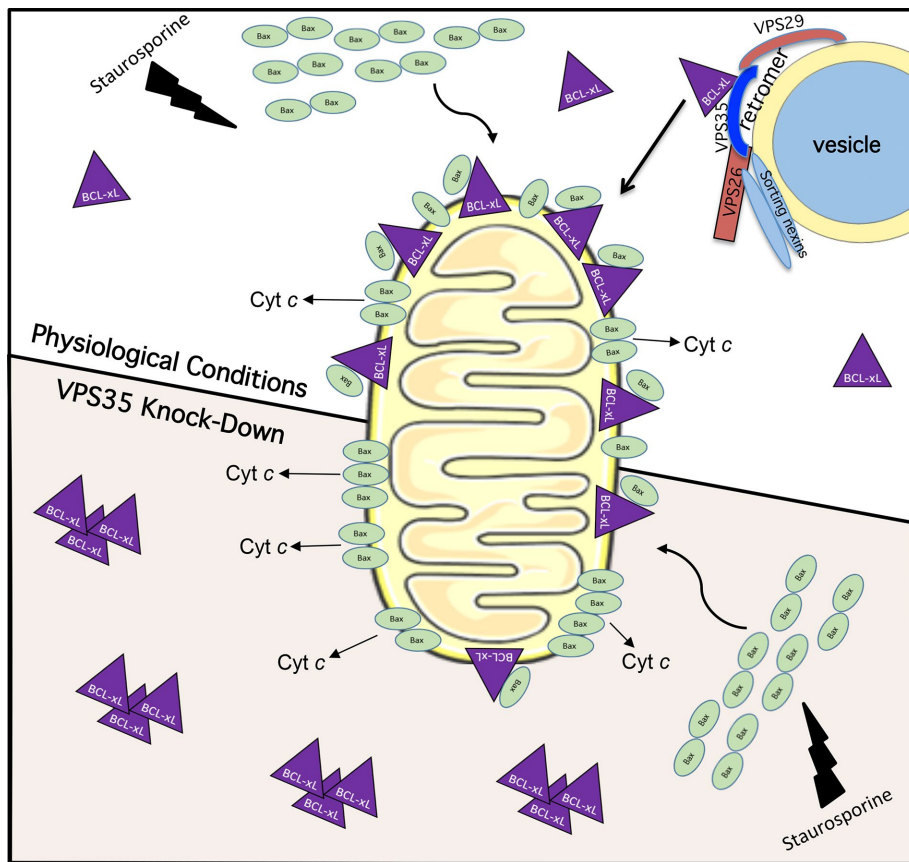


**FIGURE 5:** Model for the role of retromer in regulating Bcl-xL's translocation to the mitochondrial membrane and impact on staurosporine-induced apoptosis. Under physiological conditions (top), staurosporine treatment induces Bax translocation to the mitochondrial membrane. Because Bcl-xL is constitutively transported to the MOM, Bax pore formation is inhibited and slowed by Bcl-xL, but when sufficient Bax pore formation occurs, Cyt c is released and apoptosis occurs. Upon VPS35 knockdown (bottom), there is impaired retromer complex generation and decreased constitutive transport of Bcl-xL to the MOM. Accordingly, upon staurosporine treatment there is less inhibition of Bax by Bcl-xL, leading to more rapid Bax pore formation and an increased rate of apoptosis.

(IB, ab157220), anti-Bcl-xL (IB, IP, ab32370), anti-Bcl-xL (IF, ab26035), anti-Parp1 (IB, ab137653), and anti-Rab5 (IF, ab18211) were from Abcam; anti-DRP1 (IB, 611112) was from BD Cell Analysis; anti-MICAL-L1 (IB, IF, MBS9215151) was from MyBioSource; anti-Tom20 (IF, sc-11415) was from Santa Cruz Biotechnology; anti-EEA1 (IF, #3288) was from Cell Signaling; and anti-GAPDH-HRP (IB, HRP-60004) was from Protein Tech; donkey anti-mouse immunoglobulin (IgG) light chain-HRP (IB, 715-035-151) and mouse anti-rabbit IgG light chain-HRP (IB, 211-032-171) were from Jackson; mouse anti-rabbit IgG heavy chain-HRP (IB, ab99702) was from Abcam; donkey anti-mouse 488 (IF, A21202), donkey anti-mouse 568 (IF, 21043), goat anti-rabbit 488 (IF, A11034), goat anti-rabbit 568 (IF, A11036), and goat anti-rabbit 633 (IF, A21070) were from Molecular Probes.

**Cell culture**

The HeLa cervical cancer cell line was obtained from the American Type Culture Collection (ATCC) and grown in DMEM (high glucose) containing 10% fetal bovine serum (FBS), 1x penicillin-streptomycin (Invitrogen), and 2 mM glutamine. The immortalized retinal pigment epithelium (RPE1) cell line from the ATCC was grown in DMEM (high glucose) containing 10% FBS, 1x penicillin-streptomycin (Invitrogen), and 2 mM glutamine. The CRISPR/Cas9 HCT 116 cells lacking

endogenous Bak and Bax, with GFP-tagged Bax knocked in (GFP-Bax HCT 116) have been previously described (O'Neill et al., 2016) and were grown in McCoy's medium containing 10% FBS, 1x penicillin-streptomycin (Invitrogen), and 2 mM glutamine.

**Transfection and siRNA treatment**

Transfection of RPE1 cells for 24 h at 37°C was performed using Fugene6 (Promega) according to the manufacturer's protocol. Smart-pool ON-Target DRP1, VPS35, and MICAL-L1 oligonucleotides were obtained from Dharmacon. RPE1, HeLa, or GFP-Bax HCT 116 cells were transfected using Dharmafect 1 transfection reagent (Dharmacon) with 40 nM oligonucleotide. The efficiency of protein knockdown was measured at 72 h posttransfection by immunoblotting for each experiment.

**Plasmids**

mChr-TOMM20 was a gift from Michael Davidson (Addgene; plasmid #55146.)

**Coimmunoprecipitation**

HeLa cells were grown in 100-mm dishes until confluent. Cells were lysed with lysis buffer containing 50 mM Tris, pH 7.4, 100 mM NaCl, 0.5% Triton X-100, and 1x protease cocktail inhibitor (Millipore) on ice for 30 min. Lysates were incubated with anti-Bcl-xL, anti-VPS26, or anti-MICAL-L1 antibody at 4°C overnight. Protein G beads (GE Healthcare) were added to the lysate-antibody mix at 4°C for 4 h. Samples were then washed three times with the same lysis buffer. Proteins were eluted from the protein G beads by boiling in the presence of 4x loading buffer (250 mM Tris, pH 6.8,

8% SDS, 40% glycerol, 5% β-mercaptoethanol, 0.2% bromophenol blue) for 10 min. Eluted proteins were then identified by immunoblotting.

**Immunoblotting**

Cells were washed twice in ice-cold 1x phosphate-buffered saline (PBS) and were then scraped off plates with a rubber policeman into ice-cold lysis buffer (50 mM Tris, pH 7.4, 100 mM NaCl, 0.5% TX-100, 1x protease cocktail inhibitor [Millipore]). Protein levels of postnuclear lysates were quantified using the Bradford assay (BioRad) for equal protein level loading. For immunoblotting, 20–30 μg of protein per lysate (from either HeLa, RPE1, or GFP-Bax HCT 116 cells) was separated by SDS-PAGE. Proteins were transferred onto nitrocellulose membranes, and blocked for 30 min at room temperature in 1x PBS with 0.3% Tween (1x PBST) plus 5% nonfat dry milk. The membranes were then incubated overnight at 4°C or for 1 h at room temperature with primary antibodies diluted in 1x PBST. Membranes were then washed three times with 1x PBST and incubated at room temperature with appropriate secondary antibodies in 1x PBST for 30 min. The membranes were then washed again three times with 1x PBST, before enhanced chemiluminescence.

## Mitochondrial enrichment

HeLa cells were grown in 100-mm dishes and subject to either Mock- or VPS35-siRNA treatment for 72 h. Cells were homogenized in buffer containing 150 mM NaCl, 10 mM Tris, pH 6.8, 10 mM KCl, and 1 M sucrose. Homogenates were incubated with anti-Tom20 and rotated at room temperature for 10 min. Homogenates plus anti-Tom20 were added to Dynabeads Protein G (Invitrogen) and rotated for 10 min at room temperature. The samples were placed on the magnet and the supernatant was collected for the nonmitochondrial fraction. The Dynabeads or mitochondrial fraction was washed three times with the cell homogenization buffer. The beads and supernatant were subject to lysis in equal volumes with lysis buffer containing 50 mM Tris, pH 7.4, 100 mM NaCl, 0.5% Triton X-100, and 1× protease cocktail inhibitor (Millipore) on ice for 30 min. Loading buffer (4×) was added to each fraction and boiled for 10 min. Equal volumes were separated by SDS-PAGE and proteins were detected by immunoblotting with anti-Bcl-xL and anti-Tom20 antibodies.

## Quantification of immunoblots

The adjusted relative density of the immunoblots was measured in Fiji ImageJ according to the following protocol: [www1.med.uminn.edu/starrlab\\_deleteme/prod/groups/med/@pub/@med/@starrlab/documents/content/med\\_content\\_370494.html](http://www1.med.uminn.edu/starrlab_deleteme/prod/groups/med/@pub/@med/@starrlab/documents/content/med_content_370494.html).

## Immunofluorescence

RPE1 or GFP-Bax HCT 116 cells were treated as indicated in the text and then fixed in 4% paraformaldehyde in PBS for 10 min at room temperature. Cells were then rinsed three times in PBS. The cells were then incubated with primary antibody in PBS containing 0.5% bovine serum albumin (BSA) and 0.2% saponin for 1 h at room temperature, washed three times in PBS and then incubated with the appropriate fluorochrome-conjugated secondary antibodies diluted in PBS containing 0.5% BSA and 0.2% saponin for 30 min. Cells were washed three times in PBS and mounted in Fluoromount.

Using a Zeiss LSM800 confocal microscope with a 63×/1.4 NA oil objective, z-stack confocal images were collected. The series of images from a z-stack was then processed into a 3D projection, and a 3D snapshot was obtained using the Zeiss Zen Software. Similarly, 3D rotational videos were generated from the same 3D projections using the Zeiss Zen Software. For quantification, collected 3D snapshots were imported into Fiji ImageJ as described below.

## Colocalization quantification

Colocalization between mCh-TOMM20 and Bcl-xL, VPS26 and Bcl-xL, VPS26 and mCh-TOMM20, Bcl-xL and Rab5, or Bcl-xL and EEA1 were assessed in Fiji ImageJ. Multichannel 3D snapshots were split into separate channels. A region of interest was drawn around individual cells in one of the two channels, using the “freehand” tool. This region was then subject to the colocalization threshold plugin, and colocalization was measured and calculated.

## Nonmitochondrial Bcl-xL quantification

RPE1 cells were subject to Mock-, VPS35-, or MICAL-L1 siRNA treatment and immunostained with anti-Bcl-xL and anti-Tom20. For each treatment, the individual Bcl-xL structures that were not associated with Tom20 were counted.

## Bax activation assay

GFP-Bax HCT 116 cells were subject to either Mock- or VPS35-siRNA treatment. In the last 60 min of the siRNA treatment, the cells were treated with 1 μM staurosporine (Sigma Aldrich). Cells were

immunostained with anti-Tom20 as previously described. 250 cells per treatment were designated as either having inactive (cytoplasmic) Bax or active (punctate) Bax.

## Parp1 cleavage assay

GFP-Bax HCT 116 cells were subject to Mock- or VPS35-siRNA treatment. The cells were detached using trypsin and treated with 1 μM staurosporine for 0, 30, or 60 min. Immunoblotting was performed on the samples with anti-Parp1. The amount of Parp1 was quantified by the method described above.

## Statistics

Data from Fiji ImageJ were imported into Microsoft Excel. The mean and the SE of the mean were calculated from data obtained from three independent experiments with at least 10 images taken per treatment. Statistical significance was calculated using a Student's t test with the Vassarstats program (<http://www.vassarstats.net>).

## ACKNOWLEDGMENTS

We gratefully acknowledge funding support from the National Institute of General Medical Sciences (1R01GM123557 to S.C. and 1R01GM118437 and 1R03CA205496 to X.L.).

## REFERENCES

- Adams JM, Cory S (2018). The BCL-2 arbiters of apoptosis and their growing role as cancer targets. *Cell Death Differ* 25, 27–26.
- Arighi CN, Hartnell LM, Aguilar RC, Haft CR, Bonifacino JS (2004). Role of the mammalian retromer in sorting of the cation-independent mannose 6-phosphate receptor. *J Cell Biol* 165, 123–233.
- Barcia C, Ros CM, Annese V, Gomez A, Ros-Bernal F, Aguado-Yera D, Martinez-Pagan ME, de Pablos V, Fernandez-Villalba E, Herrero MT (2011). IFN-γ signaling, with the synergistic contribution of TNF-α, mediates cell specific microglial and astroglial activation in experimental models of Parkinson's disease. *Cell Death Dis* 2, e142.
- Basanez G, Zhang J, Chau BN, Maksiav GI, Frolov VA, Brandt TA, Burch J, Hardwick JM, Zimmerberg J (2001). Pro-apoptotic cleavage products of Bcl-xL form cytochrome c-conducting pores in pure lipid membranes. *J Biol Chem* 276, 31083–31091.
- Belmokhtar CA, Hillion J, Segal-Bendirdjian E (2001). Staurosporine induces apoptosis through both caspase-dependent and caspase-independent mechanisms. *Oncogene* 20, 3354–2362.
- Berry C, La Vecchia C, Nicotera P (2010). Paraquat and Parkinson's disease. *Cell Death Differ* 17, 1115–1125.
- Bleicken S, Classen M, Padmavathi PV, Ishikawa T, Zeth K, Steinhoff HJ, Bordignon E (2010). Molecular details of Bax activation, oligomerization, and membrane insertion. *J Biol Chem* 285, 6636–2647.
- Braschi E, Goyon V, Zunino R, Mohanty A, Xu L, McBride HM (2010). Vps35 mediates vesicle transport between the mitochondria and peroxisomes. *Curr Biol* 20, 1310–1315.
- Caplan S, Naslavsky N, Hartnell LM, Lodge R, Polishchuk RS, Donaldson JG, Bonifacino JS (2002). A tubular EHD1-containing compartment involved in the recycling of major histocompatibility complex class I molecules to the plasma membrane. *EMBO J* 21, 2557–2567.
- Choi S, Chen Z, Tang LH, Fang Y, Shin SJ, Panarelli NC, Chen YT, Li Y, Jiang X, Du YC (2016). Bcl-xL promotes metastasis independent of its anti-apoptotic activity. *Nat Commun* 7, 10384.
- Crews L, Patrick C, Adame A, Rockenstein E, Masliah E (2011). Modulation of aberrant CDK5 signaling rescues impaired neurogenesis in models of Alzheimer's disease. *Cell Death Dis* 2, e120.
- Desagher S, Osen-Sand A, Nichols A, Eskes R, Montessuit S, Lauper S, Maundrell K, Antonsson B, Martinou JC (1999). Bid-induced conformational change of Bax is responsible for mitochondrial cytochrome c release during apoptosis. *J Cell Biol* 144, 891–901.
- Eaton S (2008). Retromer retrieves wntless. *Dev Cell* 14, 4–6.
- Eskes R, Desagher S, Antonsson B, Martinou JC (2000). Bid induces the oligomerization and insertion of Bax into the outer mitochondrial membrane. *Mol Cell Biol* 20, 929–935.
- Farmer T, Naslavsky N, Caplan S (2018). Tying trafficking to fusion and fission at the mighty mitochondria. *Traffic* 19, 569–577.

- Farmer T, Reinecke JB, Xie S, Bahl K, Naslavsky N, Caplan S (2017). Control of mitochondrial homeostasis by endocytic regulatory proteins. *J Cell Sci* 130, 2359–2370.
- Farrow SN, Brown R (1996). New members of the Bcl-2 family and their protein partners. *Curr Opin Genet Dev* 6, 45–49.
- Fuchs Y, Steller H (2015). Live to die another way: modes of programmed cell death and the signals emanating from dying cells. *Nat Rev Mol Cell Biol* 16, 329–344.
- George NM, Targy N, Evans JJ, Zhang L, Luo X (2010). Bax contains two functional mitochondrial targeting sequences and translocates to mitochondria in a conformational change- and homo-oligomerization-driven process. *J Biol Chem* 285, 1384–1392.
- Gilmore AP, Metcalfe AD, Romer LH, Streuli CH (2000). Integrin-mediated survival signals regulate the apoptotic function of Bax through its conformation and subcellular localization. *J Cell Biol* 149, 431–446.
- Goping IS, Gross A, Lavoie JN, Nguyen M, Jemerson R, Roth K, Korsmeyer SJ, Shore GC (1998). Regulated targeting of BAX to mitochondria. *J Cell Biol* 143, 207–215.
- Griffiths GJ, Dubrez L, Morgan CP, Jones NA, Whitehouse J, Corfe BM, Dive C, Hickman JA (1999). Cell damage-induced conformational changes of the pro-apoptotic protein Bak in vivo precede the onset of apoptosis. *J Cell Biol* 144, 903–914.
- Guilherme A, Soriano NA, Furcinitti PS, Czech MP (2004). Role of EHD1 and EHBP1 in perinuclear sorting and insulin-regulated GLUT4 recycling in 3T3-L1 adipocytes. *J Biol Chem* 279, 40062–40075.
- Han H, Landreneau RJ, Santucci TS, Tung MY, Macherey RS, Shackney SE, Sturgis CD, Raab SS, Silverman JF (2002). Prognostic value of immunohistochemical expressions of p53, HER-2/neu, and bcl-2 in stage I non-small-cell lung cancer. *Hum Pathol* 33, 105–110.
- Hausmann G, O'Reilly LA, van Driel R, Beaumont JG, Strasser A, Adams JM, Huang DC (2000). Pro-apoptotic apoptosis protease-activating factor 1 (Apaf-1) has a cytoplasmic localization distinct from Bcl-2 or Bcl-x(L). *J Cell Biol* 149, 623–634.
- Howells CC, Baumann WT, Samuels DC, Finkielstein CV (2011). The Bcl-2-associated death promoter (BAD) lowers the threshold at which the Bcl-2-interacting domain death agonist (BID) triggers mitochondria disintegration. *J Theor Biol* 271, 114–123.
- Hsu YT, Wolter KG, Youle RJ (1997). Cytosol-to-membrane redistribution of Bax and Bcl-x(L) during apoptosis. *Proc Natl Acad Sci USA* 94, 3668–3672.
- Jeong SY, Gaume B, Lee YJ, Hsu YT, Ryu SW, Yoon SH, Youle RJ (2004). Bcl-x(L) sequesters its C-terminal membrane anchor in soluble, cytosolic homodimers. *EMBO J* 23, 2146–2155.
- Kaufmann SH, Desnoyers S, Ottaviano Y, Davidson NE, Poirier GG (1993). Specific proteolytic cleavage of poly(ADP-ribose) polymerase: an early marker of chemotherapy-induced apoptosis. *Cancer Res* 53, 3976–3985.
- Kaufmann T, Schlipf S, Sanz J, Neubert K, Stein R, Borner C (2003). Characterization of the signal that directs Bcl-x(L), but not Bcl-2, to the mitochondrial outer membrane. *J Cell Biol* 160, 53–54.
- Lee MH, Lin SR, Chang JY, Schultz L, Heath J, Hsu LJ, Kuo YM, Hong Q, Chiang MF, Gong CX, et al. (2010). TGF- $\beta$  induces TIAF1 self-aggregation via type II receptor-independent signaling that leads to generation of amyloid  $\beta$  plaques in Alzheimer's disease. *Cell Death Dis* 1, e110.
- Lee JE, Westrate LM, Wu H, Page C, Voeltz GK (2016). Multiple dynamin family members collaborate to drive mitochondrial division. *Nature* 540, 139–143.
- Li H, Alavian KN, Lazrove E, Mehta N, Jones A, Zhang P, Licznanski P, Graham M, Uo T, Guo J, et al. (2013). A Bcl-xL-Drp1 complex regulates synaptic vesicle membrane dynamics during endocytosis. *Nat Cell Biol* 15, 773–785.
- Manon S, Chaudhuri B, Guerin M (1997). Release of cytochrome c and decrease of cytochrome c oxidase in Bax-expressing yeast cells, and prevention of these effects by coexpression of Bcl-xL. *FEBS Lett* 415, 29–32.
- Naslavsky N, Caplan S (2018). The enigmatic endosome—sorting the ins and outs of endocytic trafficking. *J Cell Sci* 131, jcs216499.
- Nijhawan D, Fang M, Traer E, Zhong Q, Gao W, Du F, Wang X (2003). Elimination of Mcl-1 is required for the initiation of apoptosis following ultraviolet irradiation. *Genes Dev* 17, 1475–1486.
- Oltvai ZN, Millman CL, Korsmeyer SJ (1993). Bcl-2 heterodimerizes in vivo with a conserved homolog, Bax, that accelerates programmed cell death. *Cell* 74, 609–619.
- O'Neill KL, Huang K, Zhang J, Chen Y, Luo X (2016). Inactivation of pro-survival Bcl-2 proteins activates Bax/Bak through the outer mitochondrial membrane. *Genes Dev* 30, 973–988.
- O'Neill JW, Manion MK, Maguire B, Hockenbery DM (2006). BCL-XL dimerization by three-dimensional domain swapping. *J Mol Biol* 356, 367–381.
- Placzek WJ, Wei J, Kitada S, Zhai D, Reed JC, Pellecchia M (2010). A survey of the anti-apoptotic Bcl-2 subfamily expression in cancer types provides a platform to predict the efficacy of Bcl-2 antagonists in cancer therapy. *Cell Death Dis* 1, e40.
- Scherr AL, Gdynia G, Salou M, Radhakrishnan P, Duglova K, Heller A, Keim S, Kautz N, Jassowicz A, Elssner C, et al. (2016). Bcl-xL is an oncogenic driver in colorectal cancer. *Cell Death Dis* 7, e2342.
- Schinzl A, Kaufmann T, Borner C (2004). Bcl-2 family members: integrators of survival and death signals in physiology and pathology [corrected]. *Biochim Biophys Acta* 1644, 95–105.
- Shimizu S, Eguchi Y, Kosaka H, Kamiike W, Matsuda H, Tsujimoto Y (1995). Prevention of hypoxia-induced cell death by Bcl-2 and Bcl-xL. *Nature* 374, 811–813.
- Slomp A, Peperzak V (2018). Role and regulation of pro-survival BCL-2 proteins in multiple myeloma. *Front Oncol* 8, 533.
- Subburaj Y, Cosentino K, Axmann M, Pedrueza-Villalmanzo E, Hermann E, Bleicken S, Spatz J, Garcia-Saez AJ (2015). Bax monomers form dimer units in the membrane that further self-assemble into multiple oligomeric species. *Nat Commun* 6, 8042.
- Tabuchi M, Yanatori I, Kawai Y, Kishi F (2010). Retromer-mediated direct sorting is required for proper endosomal recycling of the mammalian iron transporter DMT1. *J Cell Sci* 123, 756–766.
- Tang FL, Liu W, Hu JX, Erion JR, Ye J, Mei L, Xiong WC (2015). VPS35 deficiency or mutation causes dopaminergic neuronal loss by impairing mitochondrial fusion and function. *Cell Rep* 12, 1631–1643.
- Tawfik K, Kimler BF, Davis MK, Fan F, Tawfik O (2012). Prognostic significance of Bcl-2 in invasive mammary carcinomas: a comparative clinicopathologic study between “triple-negative” and non-“triple-negative” tumors. *Hum Pathol* 43, 23–30.
- Tewari M, Quan LT, O'Rourke K, Desnoyers S, Zeng Z, Beidler DR, Poirier GG, Salvesen GS, Dixit VM (1995). Yama/ CPP32 $\beta$ , a mammalian homolog of CED-3, is a CrmA-inhibitable protease that cleaves the death substrate poly(ADP-ribose) polymerase. *Cell* 81, 801–809.
- Viard-Leveugle I, Veyrenc S, French LE, Brambilla C, Brambilla E (2003). Frequent loss of Fas expression and function in human lung tumours with overexpression of FasL in small cell lung carcinoma. *J Pathol* 201, 268–277.
- Wang W, Ma X, Zhou L, Liu J, Zhu X (2017). A conserved retromer sorting motif is essential for mitochondrial DLP1 recycling by VPS35 in Parkinson's disease model. *Hum Mol Genet* 26, 781–789.
- Wang W, Wang X, Fujioka H, Hoppel C, Whone AL, Caldwell MA, Cullen PJ, Liu J, Zhu X (2016). Parkinson's disease-associated mutant VPS35 causes mitochondrial dysfunction by recycling DLP1 complexes. *Nat Med* 22, 54–63.
- Wolter KG, Hsu YT, Smith CL, Nechushtan A, Xi XG, Youle RJ (1997). Movement of Bax from the cytosol to mitochondria during apoptosis. *J Cell Biol* 139, 1281–1292.
- Xie S, Reinecke JB, Farmer T, Bahl K, Yeow I, Nichols BJ, McLamarrah TA, Naslavsky N, Rogers GC, Caplan S (2018). Vesicular trafficking plays a role in centriole disengagement and duplication. *Mol Biol Cell* 29, 2622–2631.
- Xu XP, Zhai D, Kim E, Swift M, Reed JC, Volkmann N, Hanein D (2013). Three-dimensional structure of Bax-mediated pores in membrane bilayers. *Cell Death Dis* 4, e683.
- Yang E, Zha J, Jockel J, Boise LH, Thompson CB, Korsmeyer SJ (1995). Bad, a heterodimeric partner for Bcl-XL and Bcl-2, displaces Bax and promotes cell death. *Cell* 80, 285–291.
- Zhang J, Reiling C, Reinecke JB, Prislani I, Marky LA, Sorgen PL, Naslavsky N, Caplan S (2012). Rabankyrin-5 interacts with EHD1 and Vps26 to regulate endocytic trafficking and retromer function. *Traffic* 13, 745–757.